Chemical Engineering Journal 457 (2023) 141311

Contents lists available at ScienceDirect

Chemical Engineering Journal

journal homepage: www.elsevier.com/locate/cej

Enhanced remediation of cadmium-polluted soil and water using facilely prepared MnO_2-coated rice husk biomass

Yutong Zhang [a,b,1], Anyu Li [a,b,1], Lihu Liu [a,b], Xianjie Duan [a,b], Wenzhan Ge [a,b], Chengshuai Liu [c], Guohong Qiu [a,b,*]

[a] Key Laboratory of Arable Land Conservation (Middle and Lower Reaches of Yangtse River), Ministry of Agriculture and Rural Affairs, Hubei Key Laboratory of Soil Environment and Pollution Remediation, State Environmental Protection Key Laboratory of Soil Health and Green Remediation, College of Resources and Environment, Interdisciplinary Sciences Institute, Huazhong Agricultural University, Wuhan, Hubei Province 430070, China

[b] Shenzhen Branch, Guangdong Laboratory for Lingnan Modern Agriculture, Genome Analysis Laboratory of the Ministry of Agriculture, Agricultural Genomics Institute at Shenzhen, Chinese Academy of Agricultural Sciences, Shenzhen, China

[c] State Key Laboratory of Environmental Geochemistry, Institute of Geochemistry, Chinese Academy of Sciences, Guiyang, Guizhou Province 550081, China

ARTICLE INFO

Keywords:
Manganese oxides
Rice husk
Cd removal
Remediation mechanism
Hydrothermal impregnation

ABSTRACT

Metal oxide-modified biochar can effectively remediate or adsorb heavy metals in polluted soil and wastewater. However, the interaction between cellulose and hemicellulose on the surface of biochar/biomass and metal oxides is unclear, and the loading stability, adsorption capacity and mechanism of metal oxides remain to be explored. In this work, weakly crystalline birnessite (δ-MnO_2) rice husk biomass composites (MBC) were prepared via hydrothermal impregnation and then used to immobilize heavy metals in cadmium-polluted soil and wastewater. The surface of MBC was covered by sheet-like manganese oxides with a regular layered stacking structure. The adsorption of Cd(II) by MBC could be mainly attributed to monolayer chemisorption, which could achieve a maximum adsorption capacity of 115.04 mg g^{-1}. The addition of 1.0 % MBC reduced the effective Cd concentration in $CaCl_2$ extractant in the soil from 0.24 mg kg^{-1} to 0.09 mg kg^{-1}, and the highest decreasing rate reached 62.5 %. Additionally, MBC could also reduce the concentration of H_2O-leachable Cd from 22.44 μg kg^{-1} to 9.50 μg kg^{-1}. MBC facilitated the transformation of exchangeable Cd (EX-Cd) to iron-manganese bound Cd (OX-Cd) mainly comprising crystalline Mn oxide and Fe oxide. In addition, the mechanisms for MBC immobilization of Cd in polluted-soil and aqueous systems may include complexation-dominated and ion exchange-assisted processes, which contribute to a better understanding of the chemical structures and characteristics of metal oxides used to directly modify biomass. Overall, the findings indicate the possibility of applying MBC for soil and water remediation.

1. Introduction

Excessive release of heavy metals from industry and agriculture poses serious threats to the environment and human health due to their biological toxicity and accumulation [1–3]. Cadmium (Cd) can be biomagnified through the food chain due to its high mobility and accumulation, causing damage to human bones and kidneys under long-term exposure [4,5]. Soil and water are main media of Cd contamination. As a result, Cd has been identified as a carcinogen by many agencies such as the *US Environmental Protection Agency*, and the maximum contaminant level (MCL) of Cd cannot exceed 0.005 mg L^{-1}. Membrane filtration, coagulation, sedimentation and adsorption are commonly used methods in Cd-contaminated water treatment, while strategies for soil remediation mainly include bioremediation, electrochemical remediation and in situ immobilization [6]. In situ immobilization is one of the easiest methods, which is characterized by low cost, strong operability, environmental friendliness and high suitability for the treatment of contaminated soil and wastewater [7].

As an organic carbon-rich material produced from a wide range of biomass or solid wastes by pyrolysis or hydrothermal carbonization, biochar can be used to remediate polluted soil and improve soil fertility and carbon capture due to abundant functional groups and pores on its

* Corresponding author.
E-mail address: qiugh@mail.hzau.edu.cn (G. Qiu).
[1] These authors contributed equally to this work and are considered co-first authors.

https://doi.org/10.1016/j.cej.2023.141311
Received 8 November 2022; Received in revised form 25 December 2022; Accepted 3 January 2023
Available online 4 January 2023

surface [8,9]. Currently, biochar is regarded as an ideal environmental material for remediation of soil or water pollution owing to its superior removal or remediation performance for organic pollutants, heavy metals and microbial pollutants [10]. However, unmodified biochar can hardly handle pollutants effectively at high concentrations in soil or wastewater due to its low functional group activity, hydrophobicity and scarcity of adsorption sites [11]. Additionally, the carbonization process of biomass requires high temperature, which further increases the production cost. Combination of biomass with metal oxides, including iron (Fe), manganese (Mn) and magnesium (Mg), may effectively reduce the cost and improve its adsorption performance. For example, the adsorption capacity of biochar combined with Mg and Al for Cd could reach 125.34 mg g^{-1}, which is approximately 4.5-fold that of pristine biochar [12].

Manganese oxides and iron oxides are widely distributed in the environment in different structural forms, such as α-MnO_2, β-MnO_2 and δ-MnO_2. The adsorption and oxidation activity of different types of manganese oxides generally follows the order of δ-MnO_2 > β-MnO_2 > α-MnO_2, and the relatively excellent adsorption performance of δ-MnO_2 may be attributed to its intralayer octahedral vacancies [13,14]. Nagpal et al. [15] indicated that manganese oxides have excellent performance in the adsorption of cationic or anionic heavy metals and organic pollutants because of their high specific surface areas, pore structures and negative surface charges. However, manganese oxides usually have small particle sizes and high surface energies, and self-agglomeration tends to occur in micro- or nano-sized manganese oxides, affecting their performance in practical application [16]. Therefore, a combination of manganese oxides and hydrophobic matrices may effectively inhibit the self-agglomeration. For example, Maneechakr et al. [17] employed manganese dioxide-modified biochar for the adsorption of Cd (II), chromium (Cr(VI)), mercury (Hg(II)) and lead (Pb(II)), whose adsorption capacity reached 18.60, 19.92, 49.64 and 13.69 mg g^{-1}, respectively. The contribution of modified biochar to Mn loading and the remediation mechanism for heavy metals remain to be further studied. Jung et al. [18] used hydrothermal synthesis to prepare modified biochar with high affinity for copper (Cu(II)) and provided clear explanations for the regeneration and adsorption mechanisms. In addition, Liang et al. [19] demonstrated that the adsorption of Mn-modified pig manure biochar for Pb(II) and Cd(II) was highly pH-dependent, and the removal of heavy metals was dominated by specific adsorption and ion exchange.

Rice husk is a common agricultural waste with an annual global output of approximately 260 million tons [20,21]. It contains abundant cellulose, hemicellulose, trace elements and inert silica, but its utilization is currently rather limited [22]. Incineration, dumping and landfill disposal are conventional treatment for rice husk, which tend to cause a waste of resources and serious environmental pollution [12]. Preparation of biochar through carbonization of rice husk can effectively avoid the waste of resources, but the carbonization process may further increase the cost and energy consumption [10]. Lignocellulose and cellulose from the biomass are important reactants and sources of high activity sites, providing many hydroxyl and carboxyl groups for Mn modified biomass. Therefore, this study aims to prepare δ-MnO_2-loaded rice husk biomass composites (MBCx) to be used as an adsorbent by a hydrothermal process, and determine the optimal combination by varying the biomass particle size and potassium permanganate concentration. Additionally, the performance of MBCx in the adsorption of Cd from soil and water was further evaluated through isotherms, kinetics and characterization experiments. Overall, this study comprehensively analyzes the use of MBCx for the adsorption of heavy metals and provides a potential remediation agent for practical application.

2. Materials and methods

2.1. Preparation of adsorbents

Rice husk (RH) was collected from a farm in Hubei Province, washed with tap water and dried at 105 °C. The samples were crushed into powders and then sequentially passed through 0.85 mm, 0.42 mm and 0.25 mm standard sieves. For the synthesis process, 0.2 or 0.4 mol L^{-1} $KMnO_4$ and RH were reacted at 100 °C for 6 h to obtain six different gradients of the tested materials. The ratio of $KMnO_4$ and RH was calculated according to the reaction equation (the final loading matrix was rice husk powder). Specifically, the abovementioned materials were washed several times with ultrapure water, dried and passed through standard sieve with particle sizes controlled at approximately 0.85, 0.42 and 0.25 mm. The hydrothermal system was composed of 0.2 or 0.4 mol L^{-1} $KMnO_4$ solution, and the prepared materials were denoted as MBCx (x represents a number in 1 to 6), including MBC1 (0.85 mm RH, 0.2 mol L^{-1} $KMnO_4$), MBC2 (0.85 mm RH, 0.4 mol L^{-1} $KMnO_4$), MBC3 (0.42 mm RH, 0.2 mol L^{-1} $KMnO_4$), MBC4 (0.42 mm RH, 0.4 mol L^{-1} $KMnO_4$), MBC5 (0.25 mm RH, 0.2 mol L^{-1} $KMnO_4$) and MBC6 (0.25 mm RH, 0.4 mol L^{-1} $KMnO_4$). The basic physicochemical properties, such as pH values and Mn contents, are shown in Table S1. According to preexperiment, MBC5 (named as MBC hereafter) was selected as a soil remediation agent, and other MBCx were considered as control groups.

2.2. Soil remediation experiments

In this study, polluted soil was collected from the surface (0–20 cm) of a mining area in Daye city, Hubei Province. The collected soil samples were air-dried, pulverized, passed through a 0.85 mm standard sieve and mixed well. According to the 42-day remediation cycle, different doses of remediation agents were added and homogeneously mixed with the soil, and their effects on the stability and morphology of heavy metals were studied. Specifically, 50 g of soil was mixed with 0 (CK), 0.05, 0.25 and 0.5 g of the remediation agent with the corresponding content of 0, 0.1 %, 0.5 % and 1.0 %, respectively. About 30 g of distilled water was added to keep the moisture content at approximately 30 %, and the samples were kept in a constant temperature incubator for 42 d. According to the Tessier sequential extraction procedure [23], the speciation of heavy metals in soil before and after remediation can be divided into exchangeable (EX), carbonate bound (CB), iron and manganese oxide bound (OX), organic bond (OM) and residual (RS) fractions. The stability of heavy metals in the soil was further determined by $CaCl_2$ extraction [24]. Two grams of soil was weighed and mixed with 20 mL of 0.01 mol L^{-1} $CaCl_2$ solution, followed by horizontal shaking at 200 r min^{-1} for 120 min at room temperature, and the filtrate was then studied using flame atomic absorption spectrometry. H_2O was used as the leaching agent (HJ 557–2010, Chinese standard) to verify the stability of the soil after remediation in the environment. Ten grams of soil was accurately weighed and mixed with 100 mL of ultrapure water (H_2O), oscillated at 110 r min^{-1} for 8 h, and then allowed to stand for 16 h. The subsequent treatment steps were the same as those for $CaCl_2$ extraction.

2.3. Batch adsorption experiments

The equilibrium adsorption time for the aqueous adsorbent solution was determined by kinetic experiments. About 0.05 g of adsorbent was weighed and mixed with 20 mL of 200 mg L^{-1}Cd(II) solution, stirred at a 200 r min^{-1} vibration velocity for 0–90 min, filtered and tested to determine the concentration of Cd(II) in the adsorbed solution. The adsorption capacity and possible adsorption process of the adsorbent were determined by isotherm experiments. First, 25–800 mg L^{-1}Cd(II) gradient solutions were prepared with 800 mg L^{-1}Cd(II) as the mother solution and 0.01 mol L^{-1} Na_2SO_4 as the diluent electrolyte. Then, 0.05 g of adsorbent and 20 mL of the abovementioned Cd(II) gradient solution

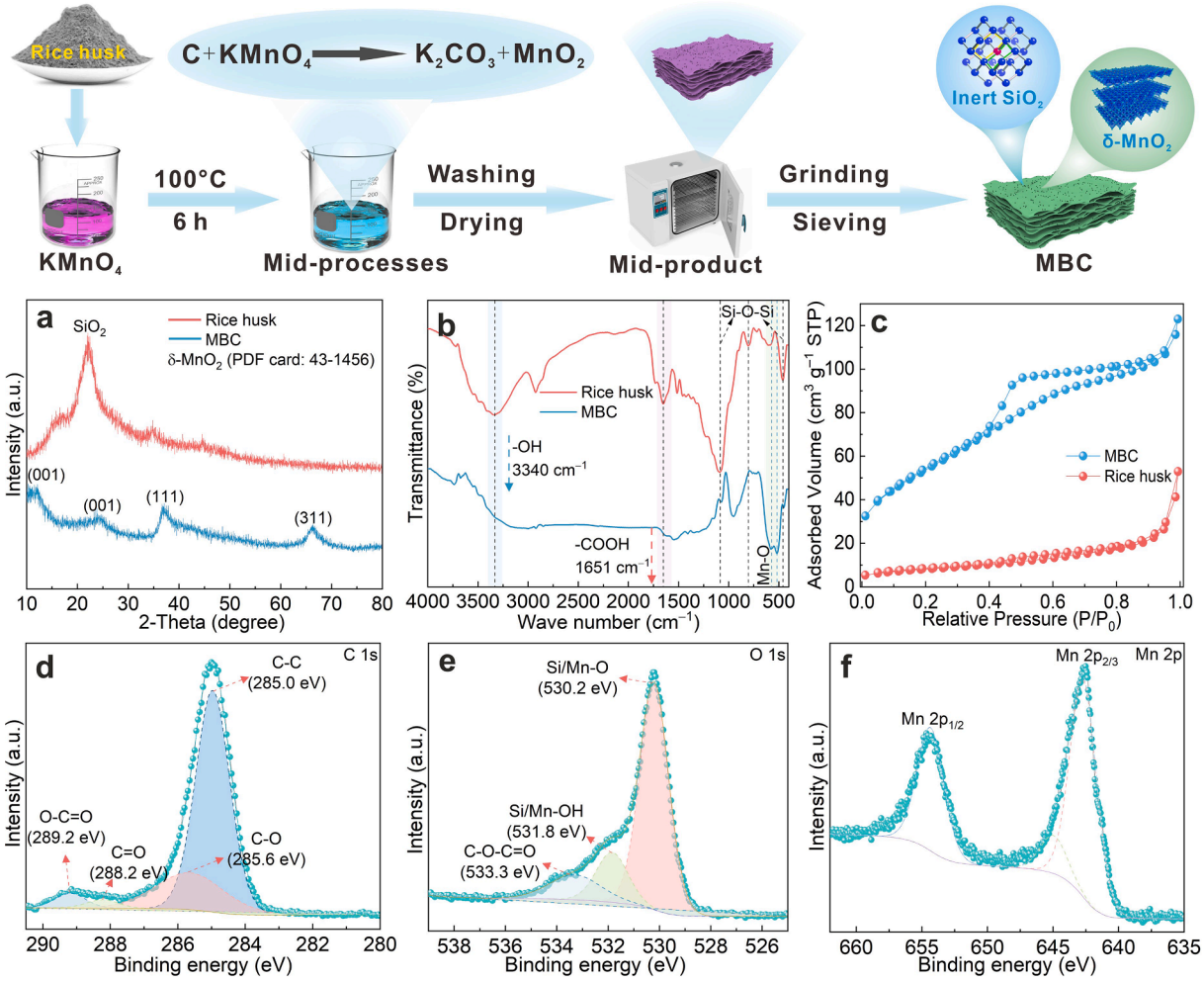

Fig. 1. XRD pattern (a), FTIR spectra (b), BET specific surface area (c), XPS survey spectra (C 1 s (d), O 1 s (e) and Mn $2p_{3/2}$ (f)).

were accurately weighed, reacted at 200 r min^{-1} vibration velocity for 120 min, filtered and used to measure the concentration of Cd(II) in the adsorbed solution. The pH of the solution is an important factor affecting the performance of the adsorbent. About 0.05 g adsorbent was weighed and mixed with 20 mL of 200 mg L^{-1}Cd(II) solution. The pH was then adjusted to the range of 1–7 with 0.01 and 0.1 mol L^{-1} H_2SO_4 and NaOH solutions, and the reaction was carried out for 120 min at a vibration velocity of 200 r min^{-1}. The subsequent treatment was consistent with the adsorption kinetics. The content of Mn in MBCx was determined with 10 % hydroxylamine hydrochloride solution. Then, 0.1 g of MBCx was weighed into a 10 mL round-bottomed centrifuge tube, followed by the addition of 2 mL 10 % hydroxylamine hydrochloride solution, which was then transferred to a 50-mL volumetric flask after the reaction, and Mn concentration in the solution was measured.

3. Results

3.1. Characteristics and properties of MBC

Fig. 1c shows the chemical composition and pore structure of MBC. The specific surface area, total pore volume and average pore size of MBC were 195.5 m^2 g^{-1}, 0.1648 cm^3 g^{-1} and 3.37 nm, respectively, all of which were higher than those of original rice husk (Table S2). This phenomenon may be attributed to the erosion of rice husk pores caused by the strong oxidant $KMnO_4$ [25]. Many studies have revealed that high porosity and specific surface area are conducive to the adsorption of heavy metals [26–28]. Table S1 shows that MBC had a higher pH value (10.49), with a Mn content as high as 43.1 %, which could provide more active sites for heavy metal immobilization. X-powder diffraction (XRD), Fourier transform infrared spectroscopy (FTIR), scanning electron microscopy-energy dispersive spectroscopy (SEM-EDS) and X-ray photoelectron diffraction (XPS) are commonly used methods to analyze material structures and surface physicochemical properties (Fig. 1a–f). The XRD pattern demonstrated the amorphous silica structure of pristine rice husk (Fig. 1a). In contrast, after $KMnO_4$ modification, there was an obvious decrease in the strength of the peak for amorphous silica, and the characteristic peaks for δ-MnO_2 crystalline planes appeared at 11.5° (0 0 1), 24.2° (0 0 1), 36.8° (1 1 1) and 66.2° (3 1 1). The δ-MnO_2 loaded on the surface of the rice husk was weakly crystalline manganese oxide, which may have a higher surface adsorption energy and activity than other types of manganese oxides [13,14,29]. Fig. 1b shows the FTIR spectrum, which was used to further analyze the functional group composition on MBC surface. MBC and pristine rice husks showed vibrational peaks at 3340 cm^{-1}, which are attributed to water (O—H stretching) [30,31], and due to the coating of Mn oxide, the vibration intensity decreased after modification. In addition, MBC showed stretching vibrations of carboxyl (–COOH) and silicon bonds (Si-O-Si) at 1651 and 1109 cm^{-1}, respectively. Notably, stretching vibration of the Mn-O bond in MBC generated a peak at approximately 500 cm^{-1}, further indicating that δ-MnO_2 was successfully loaded onto the surface of the rice husk. Therefore, modification by $KMnO_4$ changed the intrinsic properties of rice husk surface.

SEM-EDS revealed that the surface of pristine rice husk presented a rough structure and uneven distribution of surface silica particles

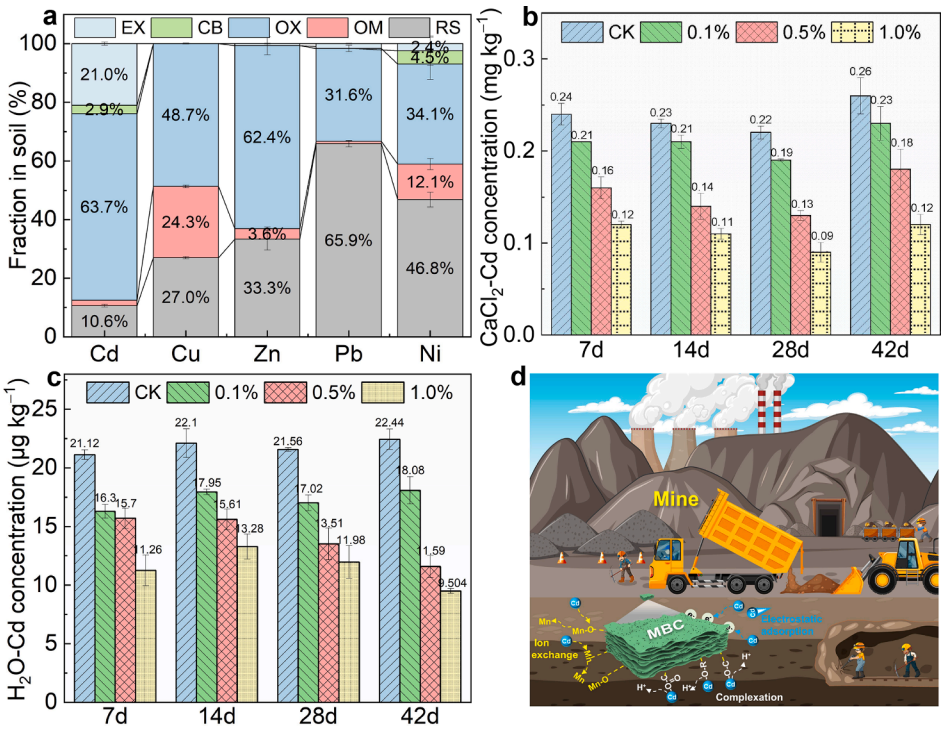

Fig. 2. Fractions of Cd, Zn, Cu, Pb, Ni in soil (a); $CaCl_2$ (b) and H_2O (c) extraction rate of Cd after 7, 14, 28 and 42 d of immobilization and possible remediation mechanisms in soil (d).

without excellent pore structures (Fig. S1). The surface of MBC exhibited sheet-like structures, which could be the characteristic microstructure of δ-MnO_2, and δ-MnO_2 was successfully attached to the surface of MBC, which showed a surface morphology similar to that reported by Lu et al. [32]. EDS also verified that the sheet-like structures were mainly composed of two elements, Mn and O. XPS was employed to further analyze the elemental composition and the amount and distribution of functional groups on MBC surface (Fig. 1d–f). Deconvolution of the C 1 s

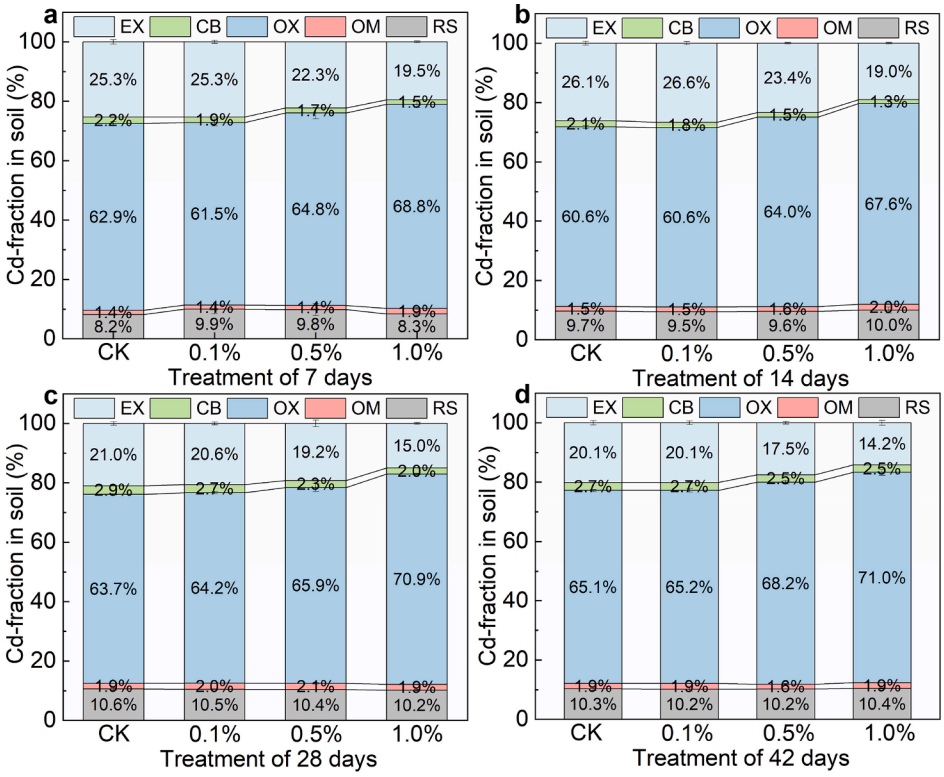

Fig. 3. Fractions of Cd after 7 (a), 14 (b), 28 (c), and 42 (d) days of immobilization by MBC. Note: EX, CB, OX, OM and RS stand for the exchangeable, carbonate bound, iron manganese oxide bound, organic bound and residual fractions, respectively.

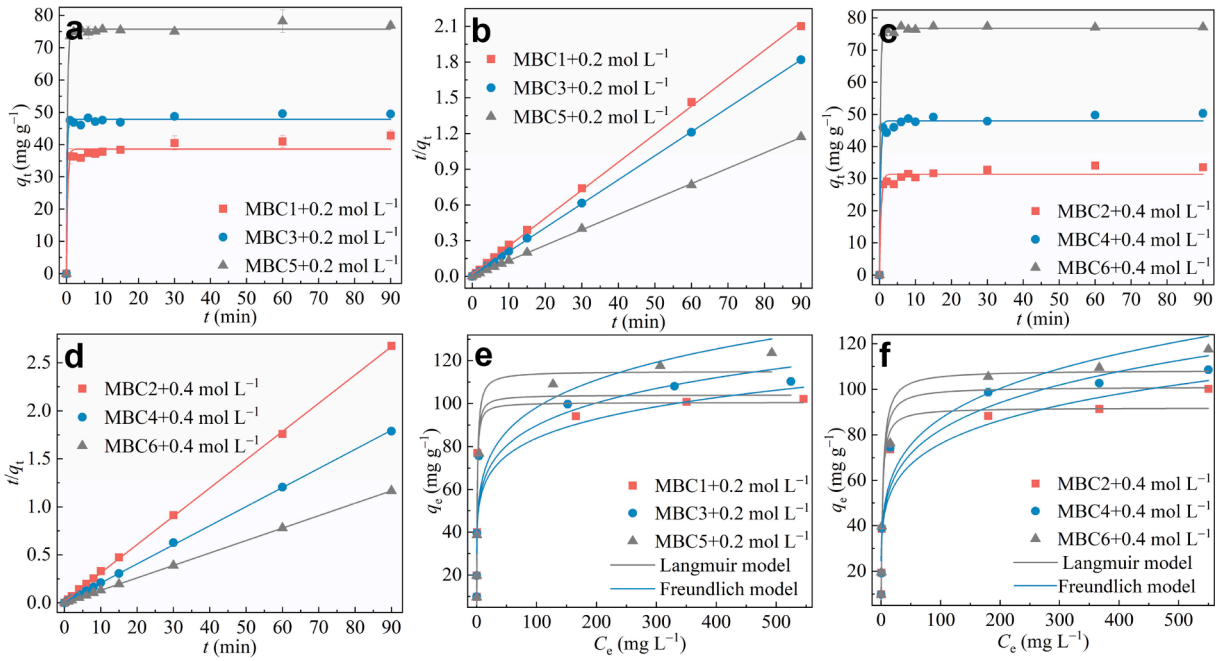

Fig. 4. Kinetics (a-d) and isotherms (e, f) fitting results of Cd(II) adsorption by MBCx.

peak generated four peaks, which are assigned to O-C═O (289.2 eV) [33], C═O (288.2 eV) [34], C—O (285.6 eV) [33] and C—C (285.0 eV), respectively [35,36]. The O 1 s spectrum was deconvoluted into three peaks assigned to C—O—C═O (533.3 eV), Si/Mn-OH (531.8 eV) and Si/Mn-O (530.2 eV), respectively [37]. The Mn 2p peak was divided into a Mn $2p_{1/2}$ and a Mn $2p_{2/3}$ doublet, which is typical for manganese species. The abundant functional groups and active sites may further enhance the adsorption capacity of MBC for heavy metals.

3.2. Remediation of heavy metal-polluted soils

The total amounts of Cd, Cu, Zn, Ni and Pb in the soil samples were 112.3, 1515.6, 1301.7, 180.7 and 419.6 mg kg^{-1}, respectively. According to the Soil Pollution Risk Control Standard for Environmental Quality of Construction Land (GB 36000–2018), the tested soil was from a Cd-contaminated site. Fig. 2a shows that the contents of exchangeable Cu, Zn and Pb were low in the Tessier sequential extraction, which followed the order of iron manganese oxide bound (OX) > residual (RS) > organic bound (OM) > carbonate bound (CB) > exchangeable (EX), OX > RS > OM > CB > EX, and RS > OX > OM > CB > EX, respectively (Figs. S2-S4). Therefore, the follow-up analysis was mainly focused on the changes in Cd morphology and leaching concentration before and after remediation. $CaCl_2$ leaching is an important indicator for environmental risks caused by changes in soil material content, which is often used to evaluate the solubility and mobility of Cd after remediation [38,39]. MBC effectively reduced the concentration of $CaCl_2$ leachable Cd ($CaCl_2$-Cd), which significantly decreased with increasing remediation cycle and addition amount of MBC (Fig. 2b). With the addition of 1.0 % MBC, the concentration of $CaCl_2$-Cd decreased from 0.24 mg kg^{-1} (average CK) to 0.12, 0.11, 0.09, and 0.12 mg kg^{-1} after 7, 14, 28, and 42 d of treatment, respectively, and the maximum leaching rate was reduced by 62.5 %. In addition, the use of H_2O as a leaching agent can also provide an evaluation index for the leaching toxicity of heavy metals (Fig. 2c). The concentration of H_2O-leachable Cd (H_2O-Cd) decreased from 22.44 μg kg^{-1} to 9.50 μg kg^{-1} with the addition of 1.0 % MBC after 42 d of remediation, while the corresponding reduction rate reached 46.7 %, 39.9 % and 44.4 % at 7, 14, and 28 d, respectively. These results demonstrated that MBC immobilization could significantly reduce the leaching concentration of Cd in the soil.

The Tessier sequential extraction was performed to further evaluate the leaching rate and the content of various forms of Cd in the soil before and after MBC remediation (Fig. 3). EX is considered to have high bioavailability because it is easily absorbed and accumulated by plants [40,41]. The bioavailability of CB, OX, OM and RS gradually decreased, and RS heavy metals are more stable in soil in the form of silicate precipitates or within the mineral lattice, and therefore are more difficult to be absorbed and utilized by organisms [42,43]. The sequential extraction results showed that the EX-Cd content of CK had slight fluctuation in different periods, and always accounted for over 20 % of the total amount, indicating that Cd in the soil is highly mobile and unstable. The Cd fractions of CK obtained by the Tessier method followed the order of OX > EX > RS > CB > OM, with OX and EX being the dominant fractions. With $CaCl_2$ leaching, the EX-Cd concentration decreased with increasing remediation time and addition amount of MBC. The addition of 0.1 % MBC did not effectively decrease the EX-Cd concentration after 42 d, indicating that a low level of MBC has little remediation effect. However, the addition of 1.0 % MBC could obviously reduce the EX-Cd from 23.1 % to 19.5 %, 19.0 %, 15.0 % and 14.2 % after 7, 14, 28 and 42 d of treatment, respectively. In the same time period, the concentration of OX-Cd increased obviously with increasing addition amount of MBC, while RS-Cd, CB-Cd and OM-Cd showed little change, indicating that Cd in the soil was mainly converted from EX-Cd to OX-Cd. In addition, Fig. 2a shows that Cu, Zn and Pb were present in the soil in relatively stable forms, whose concentrations in the soil were almost unchanged after 42 d of MBC remediation. Therefore, MBC could effectively reduce the potential toxicity and bioavailability of Cd in soil.

3.3. Adsorption performance of MBCx

Kinetics and isotherms were used to evaluate the performance of MBCx (Fig. 4). Fig. 4a and c show that at the initial stages of adsorption (0–10 min), the abundant active sites on the MBCx surface rapidly adsorbed Cd(II) in the solution. As the reaction proceeded, the adsorption tended to equilibrium due to the decrease in Cd(II) concentration in the solution and gradual depletion of adsorption sites [44]. Notably, all MBCx could rapidly adsorb Cd(II) in the solution within 10 min at a high adsorption rate. In addition, adsorption of Cd(II) by MBCx can be divided into two stages: first, Cd(II) ions rapidly diffused and were then

Table 1
Fitting parameters for the kinetics describing Cd(II) adsorption on MBCx.

Sample	Pseudo first order model			Pseudo second order model		
	$\ln(q_e\text{-}q_t) = \ln q_e\text{-}k_1 t$			$t/q_t = 1/k_2 q_e^2 + t/q_e$		
	k_1	q_e	R^2	k_2	q_e	R^2
MBC1	2.73	38.67	0.9657	0.02	42.59	0.9991
MBC3	5.02	47.87	0.9935	0.02	49.63	0.9999
MBC5	3.53	75.71	0.9978	0.01	77.22	0.9998
MBC2	2.13	31.42	0.9633	0.03	33.96	0.9997
MBC4	2.98	48.02	0.9855	0.02	50.28	0.9998
MBC6	3.91	76.73	0.9992	0.01	77.16	1.0000

Table 2
Constants of the Langmuir and Freundlich models for Cd(II) adsorption by MBCx.

Sample	Langmuir model			Freundlich model		
	$q_e = q_m k_L C_e/(1 + k_L C_e)$			$q_e = k_2 C_e^{n}$		
	k_L	q_m	R^2	k_F	n	R^2
MBC1	0.7362	100.57	0.8971	42.6457	0.1468	0.7470
MBC3	0.7962	104.07	0.9705	43.0157	0.1598	0.8965
MBC5	1.1491	115.04	0.9666	43.5214	0.1767	0.9181
MBC2	1.9351	91.95	0.9766	32.8443	0.1824	0.8853
MBC4	1.9827	102.25	0.9782	35.5506	0.1870	0.8840
MBC6	1.1821	108.18	0.9612	40.2142	0.1798	0.8988

adsorbed on MBCx surface, and then entered the interior to complex with functional groups via intraparticle diffusion [45,46]. Table 1 shows the fitting results of pseudo first order (PFO) and pseudo second order (PSO) models. The coefficient of determination (R^2) for PSO fitting was closer to 1, and the maximum adsorption capacity was equivalent to the experimental results. The PSO model further showed that chemisorption occurred between Cd(II) ions and MBCx, which plays an important role in the adsorption process [47,48].

The mechanism by which MBCx adsorb Cd(II) was further evaluated by the Langmuir and Freundlich models (Fig. 4e and f). The adsorption capacity of MBCx increased with increasing initial concentration of Cd (II). When the Cd(II) concentration was within 0–200 mg L^{-1}, the active sites on the MBCx surface could effectively adsorb Cd(II) ions, and there was a linear relationship between adsorption capacity and equilibrium concentration. With increasing Cd(II) concentration from 200 to 400 mg L^{-1}, the number of adsorption sites for Cd(II) on the surface of MBCx decreased, and competitive adsorption occurred with a relatively low reaction rate, which was also reported by Qiu et al. [49] and Li et al. [50]. With the particle size decreasing from 0.85 mm to 0.42 and 0.25 mm, the adsorption capacity showed certain improvement from 100.57 to 104.07 and 115.04 mg g^{-1} under the treatment of 0.2 mol L^{-1} $KMnO_4$ and from 91.95 to 102.25 and 108.18 mg g^{-1} under the treatment of 0.4 mol L^{-1} $KMnO_4$. The adsorption capacity of MBCx under the treatment of 0.2 mol L^{-1} $KMnO_4$ was slightly higher than that under the treatment of 0.4 mol L^{-1} $KMnO_4$. This may be because with excess $KMnO_4$, all rice husk powder participated in the reaction; the loading of MnO_2 increased with decreasing particle size; and the 0.25 mm rice husk powder had a higher loading capacity. According to the adsorption capacity of MBCx and the soil remediation efficiency in section 3.2, MBC5 (named as MBC in soil remediation) had the highest adsorption capacity (115.04 mg g^{-1}) and thus the potential to be used as a soil remediation agent. The fitting parameters in Table 2 show that both the Langmuir and Freundlich models could well fit the process for MBCx adsorption of Cd (II). However, the R^2 for the Langmuir model was higher than that for the Freundlich model, indicating that the Langmuir model could provide better fitting for the adsorption of Cd(II) by MBCx, and monolayer adsorption is the main process.

3.4. Effect of pH

The pH affects the surface charge density of MBC and adsorption of Cd(II). Cd exists mainly in the form of ions in solutions with pH lower than 7.0, and the percentages of $Cd(OH)_2$, $Cd(OH)_3^-$, $Cd(OH)^+$ and other forms of Cd gradually increase with increasing pH above 8.0 [51–54]. To avoid precipitation during experiment, the experiments in this study were conducted with a pH range of 1–7. Fig. 5a shows that the adsorption capacity of MBC for Cd(II) first increased with increasing pH, and then tended to be stable at pH > 3, at which the adsorption capacity exceeded 75 mg g^{-1}. This might be because the initial concentration of Cd was low, and Cd could be completely adsorbed by MBC at pH ≥ 4. In addition, the adsorption capacity was the lowest at the initial pH of 1; the surface of MBC was positively charged when pH < pH_{PZC}; and MBC had an electrostatic attraction effect on Cd(II) (Fig. 5b) [55–57]. On the other hand, MBC deprotonation and a high concentration of H^+ ions in the solution led to competition with Cd(II) for adsorption sites, resulting in a drop of the adsorption capacity to 18.60 mg g^{-1}. In conclusion, MBC could efficiently adsorb Cd(II) within a wide range of solution pH values. In addition, Fig. S6 shows that the recovery rate of MBC could reach about 80 % after desorption. Cd adsorbed on MBC surface basically reached desorption equilibrium after 60 min of treatment.

4. Discussion

4.1. Mechanisms for the remediation of polluted soil by MBC

In this study, MBC remediation was found to effectively reduce the bioavailability of Cd, Pb, Cu, and Zn in soil, and the effect was particularly pronounced for Cd due to the high bioavailability of the EX-Cd fraction. In general, remediation agents immobilize heavy metals in soil through complexation, precipitation, electrostatic interaction and ion exchange [58–60]. For example, Yang et al. [61] introduced some

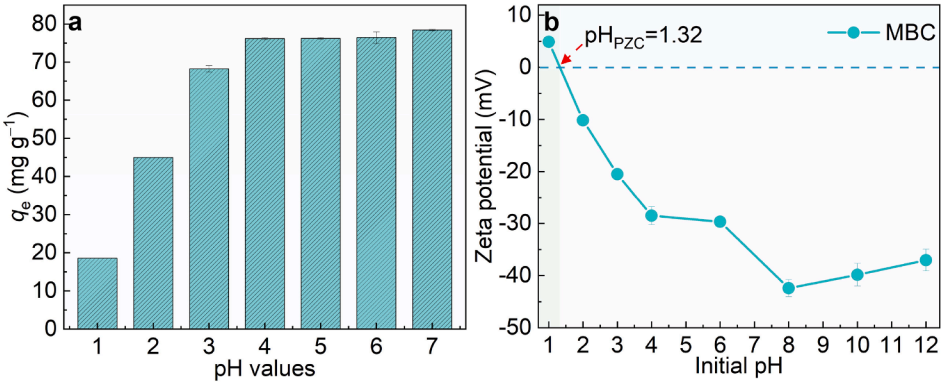

Fig. 5. Effect of pH on Cd(II) adsorption by MBC (a); and zeta potential of MBC (b).

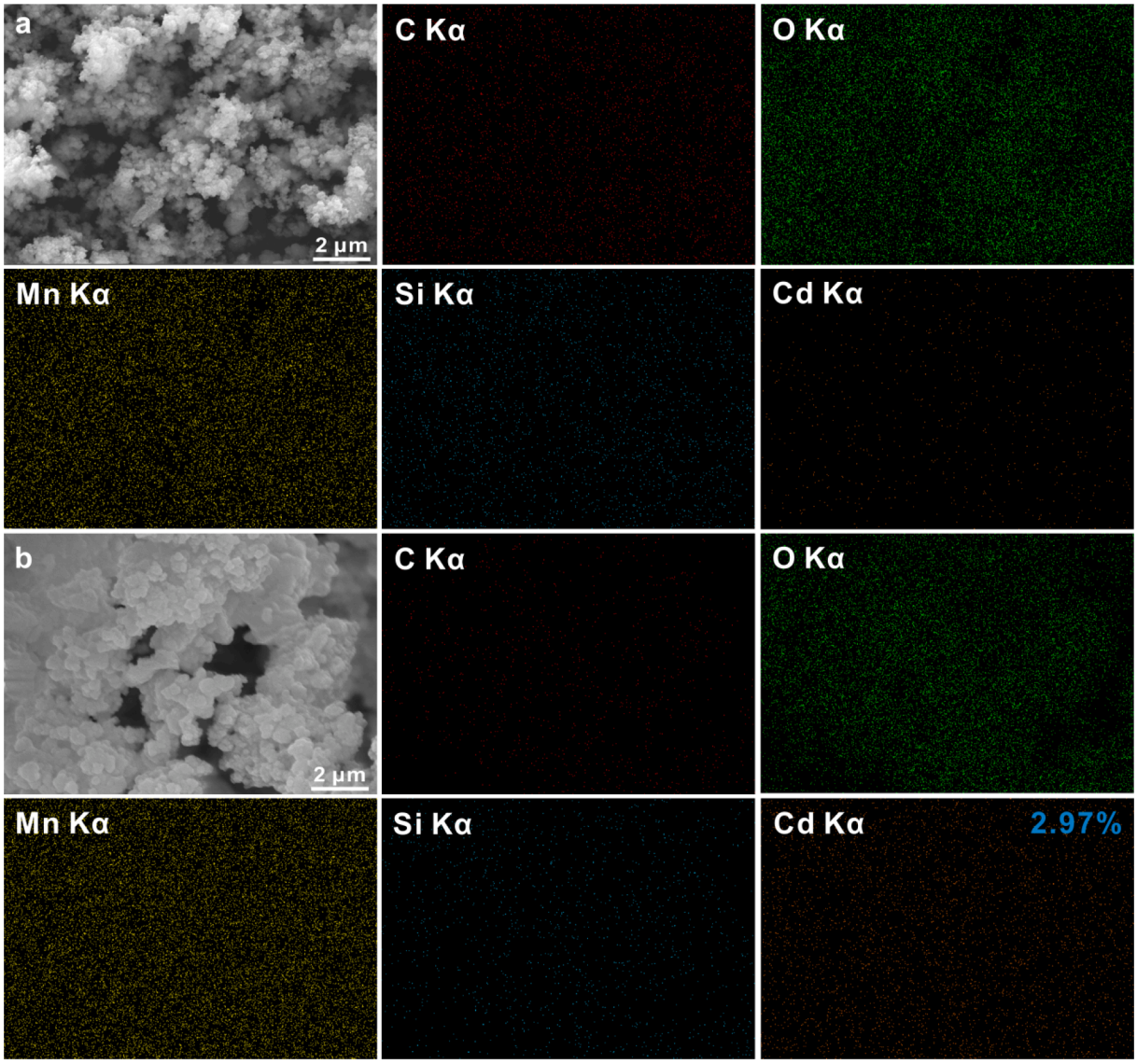

Fig. 6. SEM-EDS images of MBC before (a) and after (b) adsorption.

trace elements such as Fe and Zn into biochar as adsorption sites for Cd, which was found to promote the conversion of Cd to the iron- and manganese-bound forms. In addition, FeO could also enhance the remediation of heavy metals in soil via precipitation. Remediators can indirectly affect the speciation and distribution of heavy metals by altering the physicochemical properties of the soil. The minerals and metal oxides in MBC can increase the soil pH to certain extent (Fig. S5). An increase in OH^- concentration in the soil system can promote the conversion of metal cations such as Cd, Pb, and Cu into precipitated hydroxides, which may reduce the mobility of heavy metals in soil and thus decrease their bioavailability. In addition, alkaline conditions can inhibit the formation of As_2O_3 and improve the mobility of As, but anion mobility is not considered in this study due to the cationic nature of the soil pollutants. The surface of MBC was covered with a large amount of MnO_2, the content of which reached 43.1 %, and the surface functional groups (particularly Mn-O) promoted the complexation with Cd, which may be the main contributor to the soil remediation performance of MBC. The electronegativity and hydration radius of metal elements can also have important impacts on heavy metal immobilization. The hydration radius of Cd, Cu, Pb, and Zn is 0.426, 0.419, 0.401, and 0.430 nm, and the corresponding electronegativity is 1.69, 1.90, 2.33, and 1.65, respectively. Heavy metals with higher electronegativity are more easily adsorbed or immobilized by MBC, while those with a smaller hydration radius are more easily adsorbed [62–64]. Due to the somewhat high bioavailability of Cd, MBC may have a stronger remediation effect on Cd in soil.

Tessier sequential extraction indicated that the bioavailability of five different Cd forms followed the order of EX > CB > OX > OM > RS. Soil remediation agents can affect the forms of heavy metals in the soil in different ways and promote the transformation of EX into more stable forms. Therefore, MBC can increase the OX-Cd content by generating a more stable Mn-O-Cd form. In addition, OX-Cd is mainly composed of crystalline Mn oxide and crystalline Fe oxide, and an increase in the addition amount of MBC greatly promoted the proportion of these two forms [65] (Fig. S7). Jin et al. [66] also revealed that MnO_2 can form Mn-O-Fe-Cd inner ring complexes through oxygen-containing functional groups and Mn-O/Fe-O bonds, and the immobilization processes include complexation, ion exchange and precipitation. The contents of CB, OM and RS Cd were almost unchanged after remediation, indicating that MBC underwent a specific morphological transformation when remediating soil Cd, which provides certain guidance for subsequent improvement of the process. The proportions of Pb, Cu, and Zn were also almost unchanged after remediation, possibly due to the low contents of active forms, and the difficulty for MBC to convert small proportions of

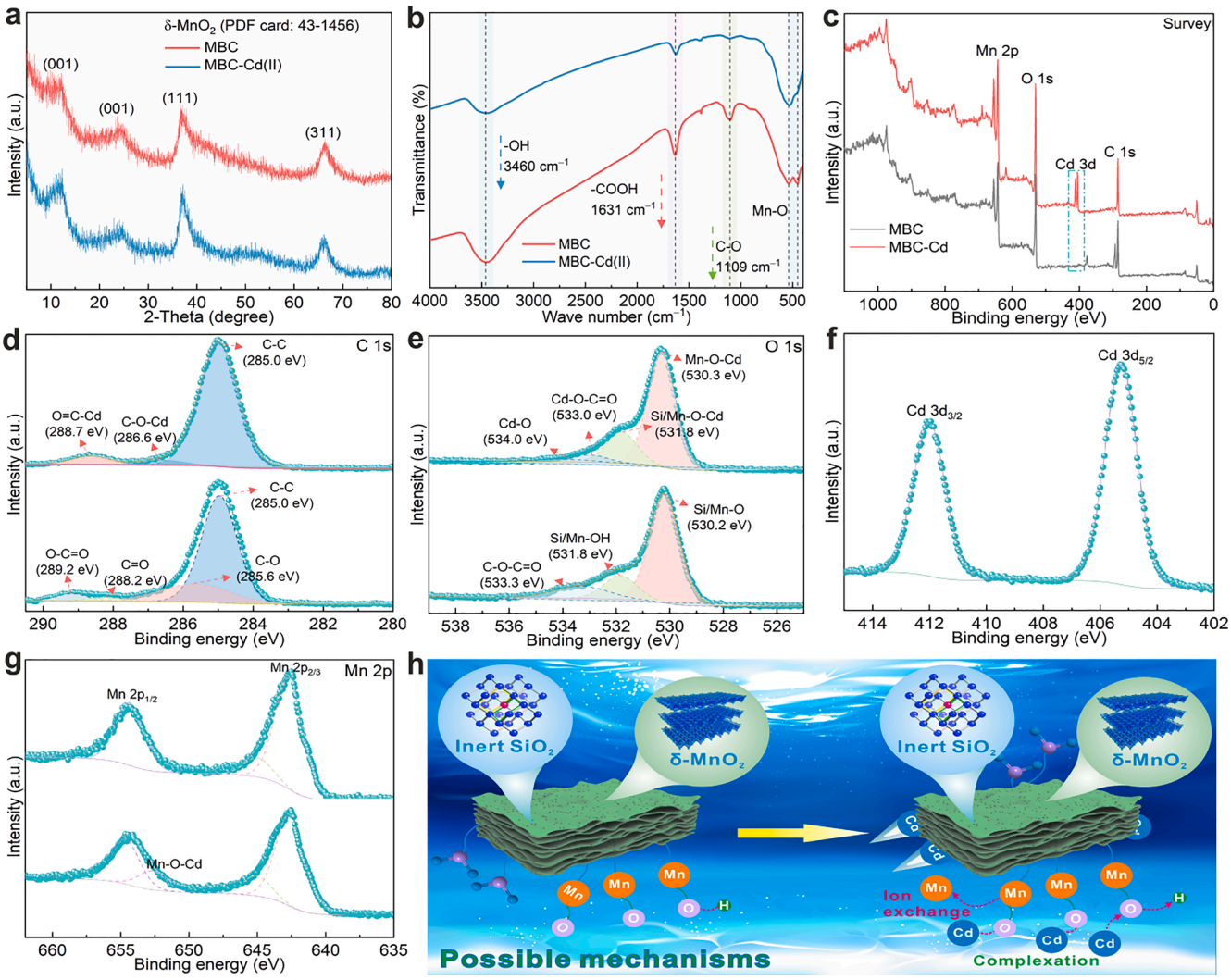

Fig. 7. XRD patterns (a), FTIR spectra (b), XPS survey spectra (full survey (c), C 1 s (d), O 1 s (e), Cd 3d (f) and Mn 2p (g)) before and after Cd(II) adsorption by MBC, and possible adsorption mechanisms for Cd(II) in wastewater (h).

EX and CB fractions into OX fraction.

4.2. Mechanisms for the wastewater remediation by MBC

Compared with pristine biochar and other Mn-modified biochars, the MBC in this study showed relatively superior Cd(II) adsorption performance. Active Mn-O bonds with strong complexing ability could adsorb Cd(II) from the solution in a very short time. Therefore, MBC may be more suitable for treatment of medium- and high-concentration heavy metals in wastewater. The Langmuir and PSO models also suggested that monolayer chemisorption is the dominant process for Cd(II) removal [67–69]. Mn-modified remediation agents usually form inner-ring complexes with heavy metals to achieve the remediation. The redox reaction of $KMnO_4$ with carbon (from the rice husk biomass) produced defects and more highly disordered carbon, decreased the aromaticity and increased the porosity and specific surface area of MBC (Fig. 1c). Therefore, MBC might rapidly adsorb Cd(II) ions through the filling effect. In addition, the possible adsorption mechanisms were further evaluated with XRD, FTIR, SEM-EDS and XPS. MBC was found to adsorb Cd(II) through complexation without changes in its own surface morphology (Fig. 6). The percentages of C, O, Si and Mn elements in pristine MBC were 20.92 %, 29.91 %, 1.28 % and 47.89 %, respectively. The EDS spectrum showed that the Cd content increased from 0 % before adsorption to 2.97 %, indicating that MBC performed effective adsorption (Fig. 6b and Fig. S8).

The XRD pattern after adsorption showed that there was no significant change in the specific crystalline faces of MBC (such as formation of new crystals, collapse and disappearance of crystal faces) (Fig. 7a). However, Cd ions were adsorbed to the surface of interlayer structure through specific complexation, leading to XRD shift after adsorption. Therefore, precipitation may not occur in the process of Cd(II) adsorption by MBC, and SEM-EDS results confirmed the stability of MBC. The high surface activity of Mn ions may promote the ion exchange with Cd ions. The vibrational peak intensity of the –COOH, -C—O and Mn-O bonds in the FTIR spectrum showed significant changes after adsorption (Fig. 7b). Complexation between the lone electron pair of -O- and Cd(II) caused changes in the –OH tensile strength [70]. The peaks for –COOH and -C—O may show decreases in intensity or even disappear upon complexation of Cd(II). It is worth noting that the Mn-O double bond is converted to a Cd-O metal bond via ion exchange. Therefore, the adsorption processes may form bidentate binuclear or polydentate complexes. Fig. 7c shows an obvious Cd 3d peak in the XPS full spectrum obtained after MBC adsorption, indicating that MBC had effectively adsorbed Cd(II). The Mn content did not decrease significantly after adsorption, and ion exchange between Mn and Cd was not the main process. The C 1 s spectrum after adsorption was deconvoluted into three peaks for O═C-Cd (288.7 eV), C—O—Cd (286.6 eV) and C—C (285.0 eV), respectively, indicating that MBC complexes with Cd

Table 3
Comparison of adsorption capacity for heavy metals by Mn-modified biochars/composites.

Adsorbents	Q (mg g^{-1})	Initial concentration (mg L^{-1})	Heavy metal	Equilibrium time	References
MBC	9.15	0–10	Pb(II)	24 h	[71]
Mn/SA-BC@nZVI	120	5–400	Cd(II)	20 min	[72]
BC-MnOx	7.62	–	Cu(II)	24 h	[73]
BC-FM	120.77	25–400	Cd(II)	30 h	[74]
CP-Fe-Mn	18.60	130–155	Cd(II)	5 min	[17]
	19.92	400–520	Pb(II)	2 min	
	13.69	100–160	Hg(II)	40 min	
MO-L-BC	248	0–60	Sb(III)	15 min	[75]
	126		Cu(II)		
MBCG	84.76	2–50	Cd(II)	20 min	[76]
	70.90		Pb(II)		
KBC	123.47	50–500	Pb(II)	100 min	[77]
MBC	115.04	25–800	Cd(II)	10 min	This work

Note: MnOx dipping biochar (MBC); Manganese-crosslinking sodium alginate modified biochar and zerovalent iron composite (Mn/SA-BC@nZVI); Manganese oxide-modified biochar (BC-MnOx); Fe-Mn oxide-modified biochar (BC-FM); Carbonized biochar powder with Fe-Mn (CP-Fe-Mn); Manganese oxide embedded in biochar (MO-L-BC); 3D MnO_2 modified biochar-based porous polyacrylamide gel (MBCG); $KMnO_4$-modified biochar (KBC).

through the O═C-O, C═O and C—O functional groups (Fig. 7d). Similarly, the O 1 s peak observed after adsorption was deconvoluted into peaks assigned to Cd-O (534.0 eV), Cd-O-C═O (533.0 eV), Si/Mn-O-Cd (531.8 eV) and Mn-O-Cd (530.3 eV), further verifying the complexation of Cd(II) by the oxygen-containing functional groups on the surface of MBC. Deconvolution of the Cd 3d peak provided a typical doublet for the Cd $3d_{3/2}$ and Cd $3d_{5/2}$ binding energy (Fig. 7f). Fig. 7f also shows that the valence state of Cd(II) remained unchanged after adsorption, and MBC removed Cd(II) from the solution through adsorption rather than oxidation or reduction processes. In addition, the Mn-O-Cd peak resulting from complexation between Mn-O and Cd further validated the above process (Fig. 7g). Therefore, the mechanisms for MBC removal of Cd(II) in aqueous systems may include complexation-dominated and ion exchange-assisted processes (Fig. 7i).

4.3. Environmental significance

The application of Mn-modified biochar to wastewater treatment has been extensively studied, but little attention has been paid to direct modification of rice husk biomass and its application to soil and water remediation. The biomass in this study is not carbonized at high temperature and will not produce secondary pollutants such as oil fume, and can be produced from a simple source via green environmental processes. Table 3 shows that the MBC preparation process is simpler than that for other Mn-modified biochars and the adsorption capacity and rate of MBC are higher. Cost benefit analysis can effectively evaluate the application potential of MBC. Based on the reaction formula, it takes 1.8 t of $KMnO_4$ and 0.25 t rice husk to prepare one ton of MBC. The price of industrial $KMnO_4$ in the current market is about approximately 1720 $ per ton. Rice husk was collected from Huangmei city, and the corresponding price and freight were about 57 and 114 $ per ton, respectively. Therefore, the preparation of one ton of MBC may consume approximately 3220 $. Adjustment of Mn loading according to the nature of the polluted site can maximize the remediation rate and reduce the production cost. In addition, this study provides an in-depth understanding of the possible mechanism for MBC removal of heavy metals from soil and wastewater as well as practical guidance for the application of remediation materials. Solutions are fast-flowing systems, and MBC can adsorb heavy metals at a higher rate in aqueous systems than in soil remediation. However, MBC will release a certain amount of Mn ions during remediation, which should be considered when using MBC to treat wastewater. On the other hand, Mn can also be used as a trace element for plant growth and competes with Cd for the absorption channels of plants. After treatment, the water reaching certain standards can be used for farmland irrigation or foliar spraying. In terms of soil remediation, MBC can initiate specific transformation of heavy metals in the soil. The heavy metals complexed by iron and manganese in the MBC remediation process can exist stably in the soil. Mn is present in the soil at high concentrations as a major element (approximately 0.4 % in this study), and the Mn released into the soil does not cause additional pollution. In addition, soil and water bodies are mostly mixed systems containing various heavy metals, and the adsorption performance of MBC for other heavy metals should be determined. Manganese oxides are also good oxidants and catalysts able to reduce the toxicity of metals (such as As and Cr) by altering their oxidation state and have promising prospects of application in catalytic degradation of organic compounds. Therefore, subsequent studies may be carried out to expand the use of MBC in environmental catalysis.

5. Conclusions

A novel remediation agent (MBC) for heavy metals was synthesized via a facile hydrothermal process. The layered stacking manganese oxides significantly improve the specific surface area and total pore volume of MBC and introduce Mn-O active groups. The enhanced remediation performance of MBC for Cd(II) can be mainly attributed to Mn-O bonds with strong complexing ability and ion exchange of Mn ions with Cd(II). Electrostatic interaction and pore filling play important roles in the immobilization of Cd(II) and may be facilitated by the lamellar structure of δ-MnO_2. The high specific surface area and excellent pore structure of MBC provide many adsorption sites for the immobilization of Cd(II), which contribute to its rapid adsorption for Cd (II) in the solution, and the maximum adsorption capacity could reach 115.04 mg g^{-1}. MBC removes Cd(II) from the solution mainly through complexation, functional group interaction and ion exchange. In addition, MBC can efficiently remove heavy metals from the soil over a short time, and metal oxygen bond complexation and functional group interaction can promote the conversion of EX-Cd to OX-Cd. Among them, strong complexation by MBC promotes the formation of OX-Cd with stable crystalline Mn oxide and crystalline Fe oxide. In conclusion, the MBC prepared in this study has high application value and may provide new implications for simultaneous remediation of heavy metal pollution in soil and water.

Declaration of Competing Interest

The authors declare that they have no known competing financial interests or personal relationships that could have appeared to influence the work reported in this paper.

Data availability

Data will be made available on request.

Acknowledgements

This work was funded by the National Key Research and Development Program of China (Grant No. 2020YFC1808503), the National Natural Science Foundation of China (Grant Nos. 42077133, 42007127 and 41877025), the Natural Science Foundation of Hubei Province of China (No: 2020CFA013), HZAU-AGIS Cooperation Fund (SZYJY2022035) and the "Light of West China" Program of the Chinese Academy of Sciences for financial support. We owe thank the public laboratory platform of the College of Resources and Environment, Huazhong Agricultural University, for their help with experimental test.

Appendix A. Supplementary data

Supplementary data to this article can be found online at https://doi.org/10.1016/j.cej.2023.141311.

References

[1] C.F. Carolin, P.S. Kumar, A. Saravanan, G.J. Joshiba, M. Naushad, Efficient techniques for the removal of toxic heavy metals from aquatic environment: A review, J. Environ. Chem. Eng. 5 (3) (2017) 2782–2799.
[2] B. Wang, Y. Zhu, Z. Bai, R. Luque, J. Xuan, Functionalized chitosan biosorbents with ultra-high performance, mechanical strength and tunable selectivity for heavy metals in wastewater treatment, Chem. Eng. J. 325 (2017) 350–359.
[3] L. Liu, A. Li, M. Cao, J. Ma, W. Tan, S.L. Suib, G. Qiu, Photoinduced self-organized precipitation in leachate for remediation of heavy metal contaminated soils, ACS EST Engg. 2 (8) (2022) 1376–1385.
[4] S. Gao, R. Zhang, H. Zhang, S. Zhang, The seasonal variation in heavy metal accumulation in the food web in the coastal waters of Jiangsu based on carbon and nitrogen isotope technology, Environ. Pollut. 297 (2022), 118649.
[5] X. Liu, L. Yin, X. Deng, D. Gong, S. Du, S. Wang, Z. Zhang, Combined application of silicon and nitric oxide jointly alleviated cadmium accumulation and toxicity in maize, J. Hazard. Mater. 395 (2020), 122679.
[6] V. Kumar, S.K. Dwivedi, A review on accessible techniques for removal of hexavalent Chromium and divalent Nickel from industrial wastewater: Recent research and future outlook, J. Clean. Prod. 295 (2021), 126229.
[7] C. Huang, H. Huang, P. Qin. In-situ immobilization of copper and cadmium in contaminated soil using acetic acid-eggshell modified diatomite. J. Environ. Chem. Eng. 8(4). (2020). 103931.
[8] M. Kamali, N. Sweygers, S. Al-Salem, L. Appels, T.M. Aminabhavi, R. Dewil, Biochar for soil applications-sustainability aspects, challenges and future prospects, Chem. Eng. J. 428 (2022), 131189.
[9] A.Y. Li, H. Deng, Y.H. Jiang, C.H. Ye, B.G. Yu, X.L. Zhou, A.Y. Ma, Superefficient removal of heavy metals from wastewater by Mg-loaded biochars: Adsorption characteristics and removal mechanisms, Langmuir 36 (31) (2020) 9160–9174.
[10] A. Li, W. Ge, L. Liu, G. Qiu. Preparation, adsorption performance and mechanism of MgO-loaded biochar in wastewater treatment: A review. Environ. Res. 212. (2022). 113341.
[11] M. Zhang, G. Song, D.L. Gelardi, L. Huang, E. Khan, O. Mašek, S.J. Parikh, Y.S. Ok, Evaluating biochar and its modifications for the removal of ammonium, nitrate, and phosphate in water, Water Res. 186 (2020), 116303.
[12] A. Li, Y. Zhang, W. Ge, Y. Zhang, L. Liu, G. Qiu. Removal of heavy metals from wastewaters with biochar pyrolyzed from MgAl-layered double hydroxide-coated rice husk: Mechanism and application. Bioresour. Technol. 347. (2022). 126425.
[13] J. Huang, S. Zhong, Y. Dai, C.-C. Liu, H. Zhang, Effect of MnO_2 phase structure on the oxidative reactivity toward bisphenol a degradation, Environ. Sci. Technol. 52 (19) (2018) 11309–11318.
[14] E. Hayashi, Y. Yamaguchi, K. Kamata, N. Tsunoda, Y. Kumagai, F. Oba, M. Hara, Effect of MnO_2 crystal structure on aerobic oxidation of 5-hydroxymethylfurfural to 2,5-furandicarboxylic acid, J. Am. Chem. Soc. 141 (2) (2019) 890–900.
[15] M. Nagpal, R. Kakkar, Use of metal oxides for the adsorptive removal of toxic organic pollutants, Sep. Purif. Technol. 211 (2019) 522–539.
[16] A. Angkaew, C. Chokejaroenrat, C. Sakulthaew, J. Mao, T. Watcharatharapong, A. Watcharenwong, S. Imman, N. Suriyachai, T. Kreetachat. Two facile synthesis routes for magnetic recoverable $MnFe_2O_4$/g-C_3N_4 nanocomposites to enhance visible light photo-Fenton activity for methylene blue degradation. J. Environ. Chem. Eng. 9(4). (2021). 105621.
[17] P. Maneechakr, S. Mongkollertlop. Investigation on adsorption behaviors of heavy metal ions (Cd^{2+}, Cr^{3+}, Hg^{2+} and Pb^{2+}) through low-cost/active manganese dioxide-modified magnetic biochar derived from palm kernel cake residue. J. Environ. Chem. Eng. 8(6). (2020). 104467.
[18] K.-W. Jung, S.Y. Lee, Y.J. Lee, Hydrothermal synthesis of hierarchically structured birnessite-type MnO_2/biochar composites for the adsorptive removal of Cu(II) from aqueous media, Bioresour. Technol. 260 (2018) 204–212.
[19] J. Liang, X. Li, Z. Yu, G. Zeng, Y. Luo, L. Jiang, Z. Yang, Y. Qian, H. Wu, Amorphous MnO_2 modified biochar derived from aerobically composted swine manure for adsorption of Pb(II) and Cd(II), ACS Sustainable Chem. Eng. 5 (6) (2017) 5049–5058.
[20] S. Ramola, T. Belwal, C.J. Li, Y.X. Liu, Y.Y. Wang, S.M. Yang, C.H. Zhou, Preparation and application of novel rice husk biochar–calcite composites for phosphate removal from aqueous medium, J. Clean. Prod. 299 (2021), 126802.
[21] H. Zhang, R. Zhang, W. Li, Z. Ling, W. Shu, J. Ma, Y. Yan, Agricultural waste-derived biochars from co-hydrothermal gasification of rice husk and chicken manure and their adsorption performance for dimethoate, J. Hazard. Mater. 429 (2022), 128248.
[22] A. Li, W. Ge, L. Liu, Y. Zhang, G. Qiu, Synthesis and application of amine-functionalized $MgFe_2O_4$-biochar for the adsorption and immobilization of Cd(II) and Pb(II), Chem. Eng. J. 439 (2022), 135785.
[23] A. Tessier, P.G.C. Campbell, M. Bisson, Sequential extraction procedure for the speciation of particulate trace metals, Anal. Chem. 51 (7) (1979) 844–851.
[24] N.S. Hailegnaw, F. Mercl, K. Pračke, J. Száková, P. Tlustoš, High temperature-produced biochar can be efficient in nitrate loss prevention and carbon sequestration, Geoderma 338 (2019) 48–55.
[25] L. Kou, J. Wang, L. Zhao, K. Jiang, X. Xu, Coupling of $KMnO_4$-assisted sludge dewatering and pyrolysis to prepare Mn, Fe-codoped biochar catalysts for peroxymonosulfate-induced elimination of phenolic pollutants, Chem. Eng. J. 411 (2021), 128459.
[26] F. Zhu, Y.-M. Zheng, B.-G. Zhang, Y.-R. Dai, A critical review on the electrospun nanofibrous membranes for the adsorption of heavy metals in water treatment, J. Hazard. Mater. 401 (2021), 123608.
[27] G. Moradi, S. Zinadini, L. Rajabi, A. Ashraf Derakhshan, Removal of heavy metal ions using a new high performance nanofiltration membrane modified with curcumin boehmite nanoparticles, Chem. Eng. J. 390 (2020), 124546.
[28] T. Hou, L. Yan, J. Li, Y. Yang, L. Shan, X. Meng, X. Li, Y. Zhao, Adsorption performance and mechanistic study of heavy metals by facile synthesized magnetic layered double oxide/carbon composite from spent adsorbent, Chem. Eng. J. 384 (2020), 123331.
[29] P. Yang, J.E. Post, Q. Wang, W. Xu, R. Geiss, P.R. McCurdy, M. Zhu, Metal adsorption controls stability of layered manganese oxides, Environ. Sci. Technol. 53 (13) (2019) 7453–7462.
[30] M.S. Alam, D. Gorman-Lewis, N. Chen, S.L. Flynn, Y.S. Ok, K.O. Konhauser, D. S. Alessi, Thermodynamic analysis of nickel(II) and zinc(II) adsorption to biochar, Environ. Sci. Technol. 52 (11) (2018) 6246–6255.
[31] Q.-C. Gong, L.-Q. He, L.-H. Zhang, F. Duan. Comparison of the NO heterogeneous reduction characteristics using biochars derived from three biomass with different lignin types. J. Environ. Chem. Eng. 9(1). (2021). 105020.
[32] T. Lu, W. Wang, L. Liu, L. Wang, J. Hu, X. Li, G. Qiu, Remediation of cadmium-polluted weakly alkaline dryland soils using iron and manganese oxides for immobilized wheat uptake, J. Clean. Prod. 365 (2022), 132794.
[33] D. Chen, X. Wang, X. Wang, K. Feng, J. Su, J. Dong, The mechanism of cadmium sorption by sulphur-modified wheat straw biochar and its application cadmium-contaminated soil, Sci. Total Environ. 714 (2020), 136550.
[34] L. Zhu, L. Tong, N. Zhao, J. Li, Y. Lv, Coupling interaction between porous biochar and nano zero valent iron/nano α-hydroxyl iron oxide improves the remediation efficiency of cadmium in aqueous solution, Chemosphere 219 (2019) 493–503.
[35] A. Li, H. Xie, Y. Qiu, L. Liu, T. Lu, W. Wang, G. Qiu, Resource utilization of rice husk biomass: Preparation of MgO flake-modified biochar for simultaneous removal of heavy metals from aqueous solution and polluted soil, Environ. Pollut. 310 (2022), 119869.
[36] S. Yang, Q. Wen, Z. Chen, Effect of KH_2PO_4-modified biochar on immobilization of Cr, Cu, Pb, Zn and as during anaerobic digestion of swine manure, Bioresour. Technol. 339 (2021), 125570.
[37] J. Liu, X. Yang, H. Liu, W. Cheng, Y. Bao, Modification of calcium-rich biochar by loading Si/Mn binary oxide after NaOH activation and its adsorption mechanisms for removal of Cu(II) from aqueous solution, Colloids Surf., A 601 (2020), 124960.
[38] J.F. Morales Arteaga, S. Gluhar, A. Kaurin, D. Lestan, Simultaneous removal of arsenic and toxic metals from contaminated soil: Laboratory development and pilot scale demonstration, Environ. Pollut. 294 (2022), 118656.
[39] S. Rodrigues, G.D. Bland, X. Gao, S.M. Rodrigues, G.V. Lowry, Investigation of pore water and soil extraction tests for characterizing the fate of poorly soluble metal-oxide nanoparticles, Chemosphere 267 (2021), 128885.
[40] H. Zhou, Z. Liu, X. Li, J. Xu, Remediation of lead (II)-contaminated soil using electrokinetics assisted by permeable reactive barrier with different filling materials, J. Hazard. Mater. 408 (2021), 124885.
[41] Y. Li, X. Tian, J. Liang, X. Chen, J. Ye, Y. Liu, Y. Liu, Y. Wei, Remediation of hexavalent chromium in contaminated soil using amorphous iron pyrite: Effect on leachability, bioaccessibility, phytotoxicity and long-term stability, Environ. Pollut. 264 (2020), 114804.
[42] S. Zhou, Y. Du, Y. Feng, H. Sun, W. Xia, H. Yuan, Stabilization of arsenic and antimony Co-contaminated soil with an iron-based stabilizer: Assessment of strength, leaching and hydraulic properties and immobilization mechanisms, Chemosphere 301 (2022), 134644.
[43] Y. Ma, L. Cheng, D. Zhang, F. Zhang, S. Zhou, Y. Ma, J. Guo, Y. Zhang, B. Xing. Stabilization of Pb, Cd, and Zn in soil by modified-zeolite: Mechanisms and evaluation of effectiveness. Sci. Total Environ. 814. (2022). 152746.
[44] A. Wang, Z. Zheng, R. Li, D. Hu, Y. Lu, H. Luo, K. Yan, Biomass-derived porous carbon highly efficient for removal of Pb(II) and Cd(II), Green Energy Environ. 4 (4) (2019) 414–423.
[45] A. Li, H. Deng, C. Ye, Y. Jiang, Fabrication and characterization of novel ZnAl-layered double hydroxide for the superadsorption of organic contaminants from wastewater, ACS Omega 5 (25) (2020) 15152–15161.
[46] J. Zhang, X. Ma, L. Yuan, D. Zhou, Comparison of adsorption behavior studies of Cd^{2+} by vermicompost biochar and $KMnO_4$-modified vermicompost biochar, J. Environ. Manage. 256 (2020), 109959.

[47] T. Chen, L. Luo, S. Deng, G. Shi, S. Zhang, Y. Zhang, O. Deng, L. Wang, J. Zhang, L. Wei, Sorption of tetracycline on H_3PO_4 modified biochar derived from rice straw and swine manure, Bioresour. Technol. 267 (2018) 431–437.
[48] Q. Shen, Z. Wang, Q. Yu, Y. Cheng, Z. Liu, T. Zhang, S. Zhou, Removal of tetracycline from an aqueous solution using manganese dioxide modified biochar derived from Chinese herbal medicine residues, Environ. Res. 183 (2020), 109195.
[49] S. Qiu, H. Zhang, D. Nie, W. Wang, G. Nie, Designing a 3D-MoS_2 nanocomposite based on the Donnan membrane effect for superselective Pb(II) removal from water, Chem. Eng. J. 452 (2023), 139101.
[50] Y. Li, S.M. Shaheen, M. Azeem, L. Zhang, C. Feng, J. Peng, W. Qi, J. Liu, Y. Luo, Y. Peng, E.F. Ali, K. Smith, J. Rinklebe, Z. Zhang, R. Li, Removal of lead (Pb^{+2}) from contaminated water using a novel MoO_3-biochar composite: Performance and mechanism, Environ. Pollut. 308 (2022), 119693.
[51] P. Liu, D. Rao, L. Zou, Y. Teng, H. Yu, Capacity and potential mechanisms of Cd(II) adsorption from aqueous solution by blue algae-derived biochars, Sci. Total Environ. 767 (2021), 145447.
[52] D. Sun, F. Li, J. Jin, S. Khan, K.M. Eltohamy, M. He, X. Liang, Qualitative and quantitative investigation on adsorption mechanisms of Cd(II) on modified biochar derived from co-pyrolysis of straw and sodium phytate, Sci. Total Environ. 829 (2022), 154599.
[53] D. Lv, X. Zhou, J. Zhou, Y. Liu, Y. Li, K. Yang, Z. Lou, S.A. Baig, D. Wu, X. Xu, Design and characterization of sulfide-modified nanoscale zerovalent iron for cadmium(II) removal from aqueous solutions, Appl. Surf. Sci. 442 (2018) 114–123.
[54] J. He, Y. Li, C. Wang, K. Zhang, D. Lin, L. Kong, J. Liu, Rapid adsorption of Pb, Cu and Cd from aqueous solutions by β-cyclodextrin polymers, Appl. Surf. Sci. 426 (2017) 29–39.
[55] Y. Wang, Z. Peng, Y. Yang, Z. Li, Y. Wen, M. Liu, S. Li, L. Su, Z. Zhou, Y. Zhu, N. Zhou, Auricularia auricula biochar supported γ-FeOOH nanoarrays for electrostatic self-assembly and pH-responsive controlled release of herbicide and fertilizer, Chem. Eng. J. 437 (2022), 134984.
[56] L. Wang, J. Wang, W. Yan, C. He, Y. Shi, $MgFe_2O_4$-biochar based lanthanum alginate beads for advanced phosphate removal, Chem. Eng. J. 387 (2020), 123305.
[57] Y.-H. Jiang, A.-Y. Li, H. Deng, C.-H. Ye, Y.-Q. Wu, Y.-D. Linmu, H.-L. Hang, Characteristics of nitrogen and phosphorus adsorption by Mg-loaded biochar from different feedstocks, Bioresour. Technol. 276 (2019) 183–189.
[58] T. Bandara, A. Franks, J. Xu, N. Bolan, H. Wang, C. Tang, Chemical and biological immobilization mechanisms of potentially toxic elements in biochar-amended soils, Crit. Rev. Environ. Sci. Technol. 50 (9) (2020) 903–978.
[59] C. Wu, D. Zhi, B. Yao, Y. Zhou, Y. Yang, Y. Zhou. Immobilization of microbes on biochar for water and soil remediation: A review. Environ. Res. 212. (2022). 113226.
[60] Y. Gao, P. Wu, P. Jeyakumar, N. Bolan, H. Wang, B. Gao, S. Wang, B. Wang, Biochar as a potential strategy for remediation of contaminated mining soils: Mechanisms, applications, and future perspectives, J. Environ. Manage. 313 (2022), 114973.
[61] T. Yang, Y. Xu, Q. Huang, Y. Sun, X. Liang, L. Wang, X. Qin, L. Zhao, An efficient biochar synthesized by iron-zinc modified corn straw for simultaneously immobilization Cd in acidic and alkaline soils, Environ. Pollut. 291 (2021), 118129.
[62] L.S. Miranda, G.A. Ayoko, P. Egodawatta, A. Goonetilleke, Adsorption-desorption behavior of heavy metals in aquatic environments: Influence of sediment, water and metal ionic properties, J. Hazard. Mater. 421 (2022), 126743.
[63] Y. Li, H. Yu, L. Liu, H. Yu, Application of co-pyrolysis biochar for the adsorption and immobilization of heavy metals in contaminated environmental substrates, J. Hazard. Mater. 420 (2021), 126655.
[64] B.-L. Zhang, W. Qiu, P.-P. Wang, Y.-L. Liu, J. Zou, L. Wang, J. Ma, Mechanism study about the adsorption of Pb(II) and Cd(II) with iron-trimesic metal-organic frameworks, Chem. Eng. J. 385 (2020), 123507.
[65] P.A. McDaniel, S.W. Buol, Manganese distributions in acid soils of the north carolina piedmont, Soil Sci. Soc. Am. J. 55 (1) (1991) 152–158.
[66] C. Jin, Z. Li, M. Huang, X. Ding, M. Zhou, C. Cai, J. Chen, Cadmium immobilization in lake sediment using different crystallographic manganese oxides: Performance and mechanism, J. Environ. Manage. 313 (2022), 114995.
[67] S.-H. Ho, Y.-D. Chen, Z.-K. Yang, D. Nagarajan, J.-S. Chang, N.-Q. Ren, High-efficiency removal of lead from wastewater by biochar derived from anaerobic digestion sludge, Bioresour. Technol. 246 (2017) 142–149.
[68] J. Liu, S. Ren, J. Cao, D.C.W. Tsang, J. Beiyuan, Y. Peng, F. Fang, J. She, M. Yin, N. Shen, J. Wang, Highly efficient removal of thallium in wastewater by $MnFe_2O_4$-biochar composite, J. Hazard. Mater. 401 (2021), 123311.
[69] S. Cheng, Y. Liu, B. Xing, X. Qin, C. Zhang, H. Xia, Lead and cadmium clean removal from wastewater by sustainable biochar derived from poplar saw dust, J. Clean. Prod. 314 (2021), 128074.
[70] Q. Li, W. Liang, F. Liu, G. Wang, J. Wan, W. Zhang, C. Peng, J. Yang, Simultaneous immobilization of arsenic, lead and cadmium by magnesium-aluminum modified biochar in mining soil, J. Environ. Manage. 310 (2022), 114792.
[71] H.-S. Lee, H.-S. Shin, Competitive adsorption of heavy metals onto modified biochars: Comparison of biochar properties and modification methods, J. Environ. Manage. 299 (2021), 113651.
[72] W. Mao, L. Zhang, Y. Zhang, Y. Guan, Simultaneous removal of arsenite and cadmium by a manganese-crosslinking sodium alginate modified biochar and zerovalent iron composite from aqueous solutions, Environ. Sci.: Nano 9 (1) (2022) 214–228.
[73] Y. Zhu, W. Fan, K. Zhang, H. Xiang, X. Wang, Nano-manganese oxides-modified biochar for efficient chelated copper citrate removal from water by oxidation-assisted adsorption process, Sci. Total Environ. 709 (2020), 136154.
[74] W.-T. Tan, H. Zhou, S.-F. Tang, P. Zeng, J.-F. Gu, B.-H. Liao, Enhancing Cd(II) adsorption on rice straw biochar by modification of iron and manganese oxides, Environ. Pollut. 300 (2022), 118899.
[75] S. Wan, L. Qiu, Y. Li, J. Sun, B. Gao, F. He, W. Wan, Accelerated antimony and copper removal by manganese oxide embedded in biochar with enlarged pore structure, Chem. Eng. J. 402 (2020), 126021.
[76] Z. Wu, X. Chen, B. Yuan, M.-L. Fu, A facile foaming-polymerization strategy to prepare 3D MnO_2 modified biochar-based porous hydrogels for efficient removal of Cd(II) and Pb(II), Chemosphere 239 (2020), 124745.
[77] H. Deng, J. Zhang, R. Huang, W. Wang, M. Meng, L. Hu, W. Gan, Adsorption of malachite green and Pb^{2+} by $KMnO_4$-modified biochar: Insights and mechanisms, Sustainability 14 (4) (2022) 2040.